ACS APPLIED ELECTRONIC MATERIALS

pubs.acs.org/acsaelm Letter

Superconducting Proximity Effect in InAsSb Surface Quantum Wells with In Situ Al Contacts

William Mayer, William F. Schiela, Joseph Yuan, Mehdi Hatefipour, Wendy L. Sarney, Stefan P. Svensson, Asher C. Leff, Tiago Campos, Kaushini S. Wickramasinghe, Matthieu C. Dartiailh, Igor Žutić, and Javad Shabani*

Cite This: https://dx.doi.org/10.1021/acsaelm.0c00269 Read Online

ACCESS | Metrics & More | Article Recommendations | Supporting Information

ABSTRACT: We demonstrate a robust superconducting proximity effect in $InAs_{0.5}Sb_{0.5}$ quantum wells grown with epitaxial Al contacts, which has important implications for mesoscopic and topological superconductivity. Unlike more commonly studied InAs and InSb semiconductors, bulk $InAs_{0.5}Sb_{0.5}$ supports stronger spin−orbit coupling and a larger *g*-factor. However, these potentially desirable properties have not been previously measured in epitaxial heterostructures with superconductors, which could serve as a platform for fault-tolerant topological quantum computing. Through structural and transport characterization, we observe high-quality interfaces and a strong spin−orbit coupling. We fabricate Josephson junctions based on $InAs_{0.5}Sb_{0.5}$ quantum wells and observe a strong proximity effect. With a contact separation of 500 nm, these junctions exhibit products I_cR_N = 270 μV and $I_{ex}R_N$ = 230 μV of normal resistance R_N, critical current I_c, and excess current I_{ex}. Both of these quantities demonstrate a robust and long-range proximity effect with highly transparent contacts.

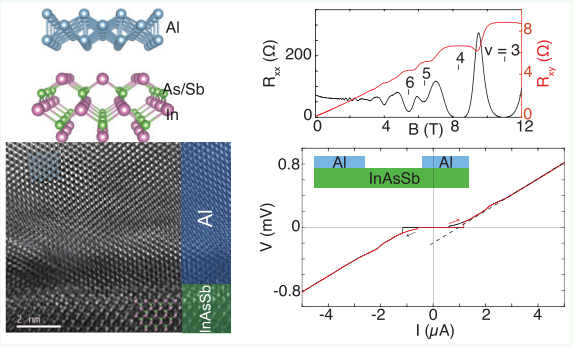

KEYWORDS: *proximity effect, superconductivity, surface quantum well, molecular beam epitaxy, magnetotransport, Josephson junction*

A given material can be transformed through proximity effects, whereby it acquires correlations from its neighbors, for example, becoming superconducting or magnetic. Such proximity effects not only complement the conventional methods of designing materials by doping or functionalization but can also overcome their various limitations and enable novel states of matter.[1] A striking example of this approach is semiconductors with strong spin−orbit coupling (SOC) and a large *g*-factor, in proximity to conventional superconductors. Such structures are predicted to support topological superconductivity with exotic quasiparticle excitations including Majorana bound states (MBS), which hold promise for fault-tolerant quantum computing.[2,3] Through braiding (exchange) of MBS, it is possible to reveal their peculiar non-Abelian statistics and implement fault-tolerant quantum gates.[4]

Most efforts to realize MBS have been focused on one-dimensional (1D) systems, typically relying on proximitized InAs and InSb nanowires in an applied magnetic field (see recent review articles refs 5 and 6 and references therein). However, their geometry has inherent difficulties to implement braiding and imposes strong constraints on material parameters to achieve topological superconductivity, usually inferred from observation of a quantized zero-bias conductance peak. Instead, to overcome these limitations, there is a growing interest in 2D platforms of proximitized semiconductors, which would also support topological superconductivity.[7] These advantages have recently been demonstrated in planar Josephson junctions[8−10] where the phase transition between trivial and topological superconductivity can be tuned using gate voltages and the superconducting phase. This allows for more complicated networks that could support fusion, braiding, and large-scale Majorana manipulation.

Our experiments on $InAs_{0.5}Sb_{0.5}$-based two-dimensional electron gas (2DEG) are complemented by numerical studies of its electronic structure, Rashba SOC, and *g*-factor. From previous work, it is reported that $InAs_{0.5}Sb_{0.5}$ can exhibit significantly larger spin-splitting,[3] compared to InAs or InSb, in which transport properties have been extensively explored. The bulk *g*-factor of $InAs_{0.5}Sb_{0.5}$ is expected to reach up to −120 and exhibit an SOC almost an order of magnitude stronger than that of InAs.[11] We find that the *g*-factor is suppressed in

Received: March 31, 2020
Accepted: June 23, 2020
Published: June 23, 2020

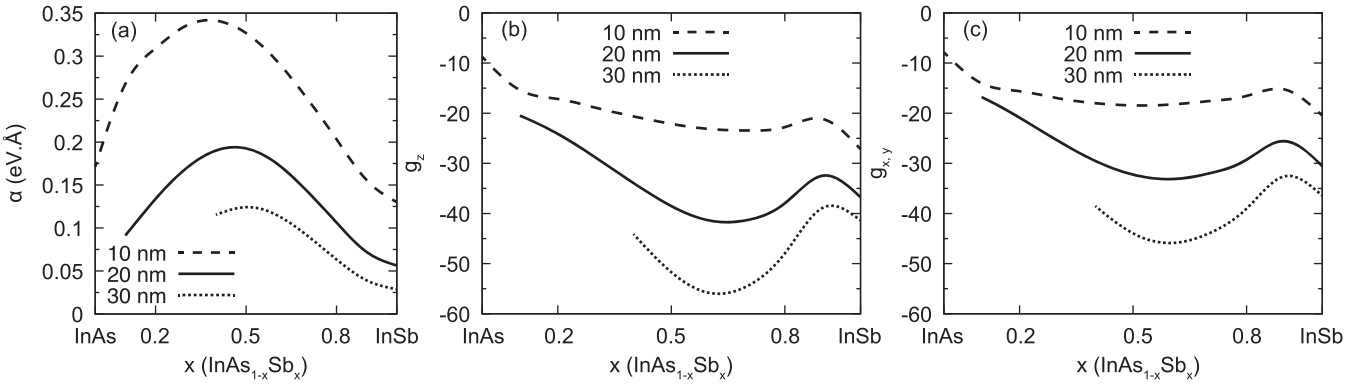

Figure 1. Numerical calculations using the standard eight-band $\vec{k}\cdot\vec{p}$ method. Legends indicate quantum well thickness. (a) Rashba spin−orbit coupling parameter, α, for the $InAs_{1-x}Sb_x$ quantum well. (b,c) g-Factor for the $InAs_{1-x}Sb_x$ quantum well. There is a nonmonotonic behavior in both α and the g-factor going from pure InAs to pure InSb. By increasing the quantum well size, α decreases, while the g-factor increases in magnitude.

narrow quantum wells, while the linear term in spin−orbit coupling decreases as the quantum well width is increased.

We use a standard eight-band $\vec{k}\cdot\vec{p}$ method[12] to calculate the sub-band structure of the surface $InAs_{0.5}Sb_{0.5}$ QW. The quantum confinement along the growth direction was addressed by using the finite difference method with a discretization step of 0.5 nm, which is sufficient to achieve convergence. For computational efficiency, we neglect the impact of the metal−semiconductor interface by modeling it as a hard-wall barrier acting as a confinement layer for the carriers. The material parameters were taken from ref 13, while the bowing parameter for the $InAs_{0.5}Sb_{0.5}$ alloy was taken from ref 14.

Since the system has broken inversion symmetry, the energy dispersion, $\varepsilon_{n,\sigma}(k_z)$, is spin-split due to the Rashba SOC. In Figure 1a we show the computed Rashba SOC parameter, α, for the first conduction sub-band, computed as the linear slope of the energy difference $\Delta E = \varepsilon_{1,\sigma}(k_z) - \varepsilon_{1,\sigma'}(k_z)$, is very close to the Γ-point.[15] In order to understand the quantum confinement as well as the effect of the alloy composition, x, we consider three $InAs_{1-x}Sb_x$ layer sizes and vary the composition x from pure InAs to pure InSb. The gap at the $InAs_{1-x}Sb_x/In_{0.37}Al_{0.63}Sb$ interface is a broken one, i.e., the valence band edge is higher in energy than the conduction band edge and by increasing the $InAs_{1-x}Sb_x$ layer size, the confined states' energies cross each other. In this situation, no spin-splitting was computed, since the conduction and valence sub-bands crossed. Furthermore, the trend that the smaller the $InAs_{1-x}Sb_x$ layer size, the larger the Rashba parameter is due to the fact that the electron has a higher probability to be found near the interfaces than in the middle of the layer. Indeed, as we reduce the $InAs_{1-x}Sb_x$ layer size, the Rashba SOC parameter becomes larger. We found that the highest value is around α = 0.35 eVÅ for the 10 nm $InAs_{0.4}Sb_{0.6}$ layer, α = 0.2 eVÅ for the 20 nm $InAs_{0.5}Sb_{0.5}$ layer, and α = 0.12 eVÅ for the 30 nm $InAs_{0.6}Sb_{0.4}$ layer. Our calculation does not include electrostatic self-consistency, and since Fermi-level pinning, which one can expect to be composition dependent, would increase the asymmetry of the structure,[16] our calculation provides a minimum for the spin−orbit coupling strength and may not capture its full composition dependence.

The g-factor was computed using second order Löwdin partitioning.[17,18] In the bulk limit, it converges to the Roth formula for an effective g-factor

$$g^* = 2\left(1 - \frac{m_e}{m^*}\frac{\Delta_{SS}}{3E_g + 2\Delta_{SS}}\right) \quad (1)$$

where Δ_{SS} is the spin−orbit-splitting of the valence bands, and E_g is the energy gap, while m_e and m^* are the free and effective electron masses, respectively. In Table 1, we show the bulk g-factor for the $In_{0.37}Al_{0.63}Sb$ barrier, InAs, InSb, and three selected $InAs_{1-x}Sb_x$ compositions. As we increase the composition, x, the band gap of the material decreases, and since the main contribution to the g-factor comes from $1/E_g$,[18] we obtain the largest g-factor values for compositions varying from x = 0.4 to x = 0.6.

Table 1. Bulk g-Factor Using Roth Formula

compound	g^*
$In_{0.37}Al_{0.63}Sb$	−4.65
InAs	−14.61
$InAs_{0.6}Sb_{0.4}$	−70.86
$InAs_{0.5}Sb_{0.5}$	−99.08
$InAs_{0.4}Sb_{0.6}$	−116.82
InSb	−49.23

With quantum confinement, the g-factor is typically lower than the corresponding bulk value. This trend can also be inferred from eq 1, since for a highly confined system, the effective band gap increases (as the energy difference from the conduction to valence band also increases). We show the calculated g-factor for a confined system along the growth direction, g_z in Figure 1b, as well as perpendicular to the growth direction, $g_{x,y}$ in Figure 1c. Due to the quantum confinement and SOC, the g-factor is anisotropic, i.e., $\Delta_g = g_{x,y} - g_z \neq 0$,[19] with g_z being larger in magnitude than $g_{x,y}$. Moreover, following the trend of the Roth formula in eq 1, as we increase the size of the $InAs_{1-x}Sb_x$ layer, the g-factor also increases. We found that the largest g-factor occurs for a 30 nm $InAs_{0.4}Sb_{0.6}$ QW and exceeds previous experimental results for a 30 nm InSb QW, which found in-plane $|g_{x,y}| = 26$ and out-of-plane $|g_z| = 52$.[20] The above calculations show that there is a sweet spot in terms of QW width where the g-factor and SOC are both strong. Motivated by this fact, we focus the rest of our studies on 20 nm QWs.

Molecular beam epitaxy (MBE) growth of large-area $InAs_{0.5}Sb_{0.5}$ surface QWs in epitaxial contact to aluminum films can form the basis for combining the proximity effect

https://dx.doi.org/10.1021/acsaelm.0c00269
ACS Appl. Electron. Mater. XXXX, XXX, XXX−XXX

with high g-factor, strong SOC systems. Growth of semiconductor $InAs_{0.5}Sb_{0.5}$ is rather difficult, since there is no insulating lattice-matched substrate immediately available. In this work, we utilized the process of compositional grading to produce a substrate interface with the required lattice constant. This enables growth of bulk, unstrained $InAs_{1-x}Sb_x$ of arbitrary composition onto GaSb without relaxation at the interface, as previously reported.[22,23] Following earlier work, our samples have a 2.6 μm GaInAlSb compositional grade followed by a 0.25 μm $In_{0.37}Al_{0.63}Sb$ virtual substrate (VS) and a 200 Å $InAs_{0.5}Sb_{0.5}$ layer. Figure 2c shows a schematic of the layers,

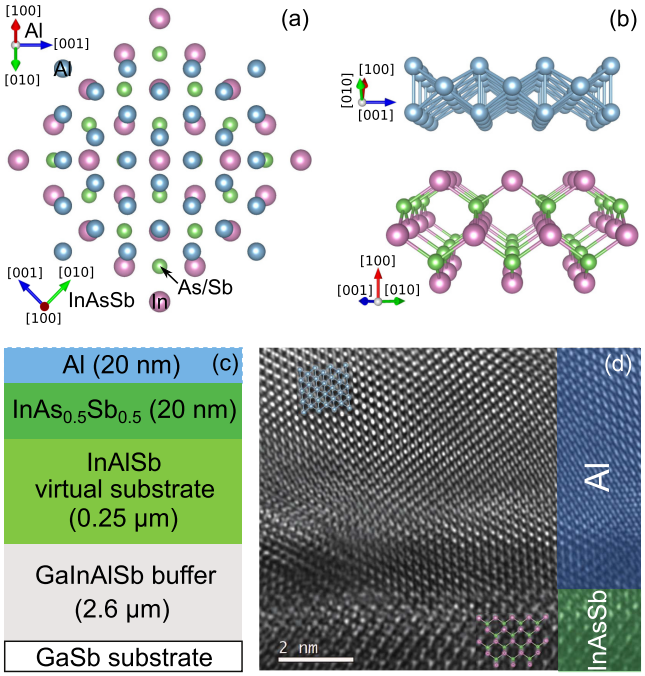

Figure 2. (a) Unstrained Al on $InAs_{0.5}Sb_{0.5}$ with respective lattice constants 4.05 and 6.27 Å, projected onto the plane of growth. (b) Three-dimensional rendering of the Al–$InAs_{0.5}Sb_{0.5}$ interface from the perspective of the transmission electron microscope image below. (c) Layer diagram of the $InAs_{0.5}Sb_{0.5}$ surface quantum well with an Al contact. (d) Cross-sectional transmission electron microscope image of the Al–$InAs_{0.5}Sb_{0.5}$ interface along the ⟨110⟩ zone axis with unstrained Al and $InAs_{0.5}Sb_{0.5}$ lattices overlaid.[21]

while Figure 2a shows a top view of the unstrained face-centered cubic Al lattice superimposed on the unstrained zincblende $InAs_{0.5}Sb_{0.5}$ lattice. We grew the sample by solid-source molecular beam epitaxy in a modular Gen II system with the As and Sb delivered by valved cracker sources. Except during the Al layer deposition, the substrate temperature was measured with a K-space BandiT system operating in pyrometry mode. Measurements of (004) triple-axis X-ray diffraction allowed us to verify the composition of the VS. We cannot examine the $InAs_{0.5}Sb_{0.5}$ layer, since it is too thin relative to the VS and the compositional grade, but test structures with thicker $InAs_{0.5}Sb_{0.5}$ layers were grown with this recipe, and their composition was verified by X-ray diffraction.

For samples with Al, after the top $InAs_{0.5}Sb_{0.5}$ layer was grown, all shutters were closed, and the sources were cooled to idling temperatures (around 300–400 °C). The residual gases were pumped overnight, allowing the background pressure in the chamber to reach the 10^{-11} Torr range. The next day, the sample was pointed toward the cryo-shroud for 2 h and 40 min, allowing it to fall below 0 °C. We deposited a 200 Å layer of Al onto the $InAs_{0.5}Sb_{0.5}$ surface at a growth rate of 0.09 Å/s. In this work, we present data from nominally identical structures, one with and one without an in situ Al layer.[24] Figure 2d shows a cross-sectional transmission electron microscope image of the interface between the $InAs_{0.5}Sb_{0.5}$ and Al layers along the ⟨110⟩ zone axis, while Figure 2b shows a 3D rendering of the interface from the same perspective. The substrate and $InAs_{0.5}Sb_{0.5}$ are oriented along a ⟨001⟩ growth direction. The Al film consists of large domains predominately aligned along ⟨110⟩, tilted ∼4° from the interfacial plane. The high-resolution images of this region and numerous others show that the d-spacing of the growth direction planes is 2.9 Å, corresponding to that for Al along ⟨110⟩. The orientation relationships of the crystal planes and the FFT pattern correspond to Al examined at a zone axis with a ⟨110⟩ growth direction.

We studied the magnetoresistance of the $InAs_{0.5}Sb_{0.5}$ surface 2DEG grown without Al in a 4 × 4 mm van der Pauw geometry, using indium solder to secure 1 mil diameter gold wires to the four corners of the sample. Samples without Al are used in magnetotransport measurements of the $InAs_{0.5}Sb_{0.5}$ layer to avoid shorting the probe electrodes through the Al layer. If necessary, transport in samples grown with Al may be studied by first removing the Al layer using a Transene Type D Al etchant. Empirically, we observe chemical processing and surface treatment result in increase of carrier density and decrease of mobility in the 2DEG; however, we have not performed a systematic study of such effects. Here, we present transport data from samples grown without Al. Measurements were performed at T = 1.5 K using standard lock-in techniques and ac excitations I_{ac} = 50 nA–1 μA at frequencies below 100 Hz. We find mobilities of μ = 25 000 cm^2/(V s) at a carrier density $n = 8 \times 10^{11}$ cm^{-2}.

In the presence of strong SOC, the Shubnikov-de Haas oscillations are expected to contain two frequencies, signaling two Fermi surfaces. The appearance of an amplitude-modulated beat in the oscillations followed by a node, as shown in Figure 3a, suggests occupation of two spin sub-bands. Figure 3b shows the Fourier transform of these oscillations over the 1 to 5 T range. There are three clear peaks, which indicate spin-split sub-bands with frequencies f_+ = 17.2 T, f_- = 14.2 T and a peak for the total frequency at f_{tot} = 33 T. The densities can be directly calculated from $n_\pm = qf_\pm/h$ where q is the electron charge and h is Planck's constant. We obtain $n_+ = 4.2 \times 10^{11}$ cm^{-2} and $n_- = 3.4 \times 10^{11}$ cm^{-2} with $n_{tot} = 7.6 \times 10^{11}$ cm^{-2}, which agrees with the Hall data shown in Figure 3c. This suggests the spin-split sub-band separation is very large as expected for $InAs_{0.5}Sb_{0.5}$. If this splitting were all due to the linear Rashba SOC term, we would obtain its parameter as $\alpha = (\Delta n\hbar^2/m^*)\sqrt{\pi/[2(n_{tot} - \Delta n)]} = 0.8$ eVÅ, where $\Delta n = |n_+ - n_-|$, assuming a band mass of $m^* = 0.011m_e$ at 50% composition.[25] Our $\vec{k} \cdot \vec{p}$ calculation for this QW width predicts α = 0.2 eVÅ, which is lower than the α = 0.8 eVÅ estimated from extracted parameters, suggesting there are contributions from Dresselhaus SOC terms in Sb compounds.[26] We also note that a Schrödinger-Poisson calculation for our 20 nm QW showed one electronic sub-band is occupied.

We further characterize the superconducting proximity effect in a Josephson junction (JJ) on an $InAs_{0.5}Sb_{0.5}$ 2DEG with epitaxial Al contacts, as depicted schematically in Figure 4a.

https://dx.doi.org/10.1021/acsaelm.0c00269
ACS Appl. Electron. Mater. XXXX, XXX, XXX–XXX

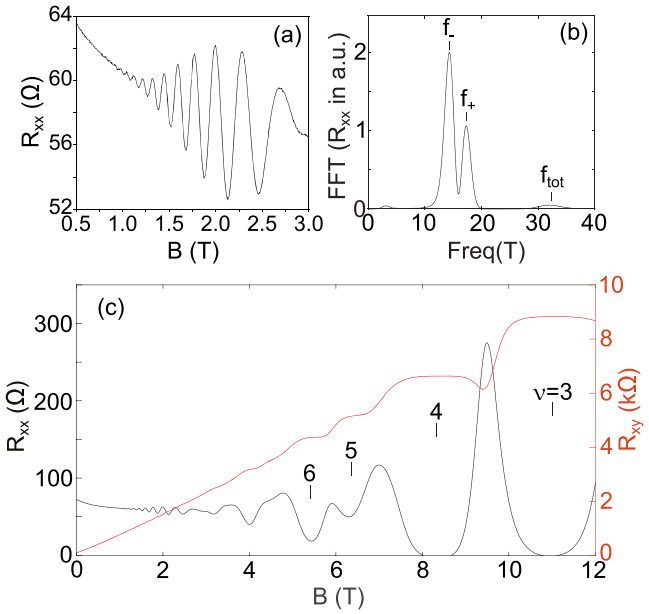

Figure 3. Transport measurements of a near-surface $InAs_{0.5}Sb_{0.5}$ quantum well grown without Al exhibit a carrier density $n = 8 \times 10^{11}$ cm^{-2} and mobility $\mu = 25 \times 10^3$ cm^2/(V s) at 1.5 K. (a) Beating of the longitudinal resistance at low magnetic field (a selected region of plot (c)). (b) Fast Fourier transform of the longitudinal resistance in the range 1−5 T. (c) Longitudinal (black) and Hall (red) resistance shown as a function of magnetic field.

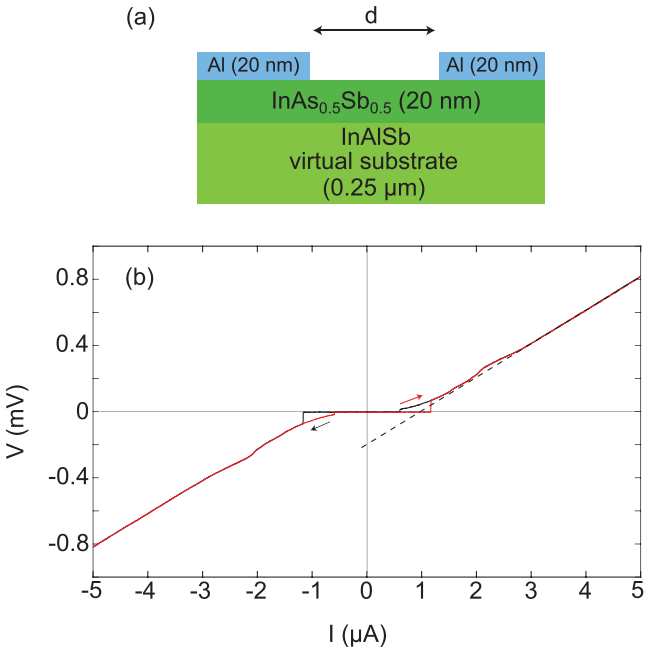

Figure 4. (a) Schematic of the Josephson junctions on $InAs_{0.5}Sb_{0.5}$ with separation d between Al contacts. (b) Current−voltage characteristics of the d = 500 nm junction at 20 mK. The dashed line is an extrapolated linear fit of the region $eV > 2\Delta_{Al}$.

We fabricated Josephson junctions via electron beam lithography followed by selective wet etching (Transene Type D) to remove a thin strip of Al. The junction is 4 μm wide and has a 500 nm length separation between the superconducting electrodes. Measurements were performed in a dilution fridge with a mixing chamber temperature of 7 mK and an estimated electron temperature of 20 mK. We used a four-point measurement configuration and standard dc bias techniques whereby a pair of contacts are used to drive current across the junction to ground, while an adjacent pair measures the concomitant voltage drop across the junction. The $I-V$ characteristic of the junction is shown in Figure 4b. The voltage drop across the junction is zero (the supercurrent) up to a critical value of driving current denoted the critical current, I_c = 1.16 μA.

The quality of the device can be characterized by a study of the I_cR_N and $I_{ex}R_N$ products, where R_N is the normal resistance of the JJ. The excess current I_{ex} is the difference between the measured current through the junction and the expected current based on the junction's R_N. This occurs due to Andreev reflections and depends primarily on interface transparency. The critical current I_c is the amount of current that can be carried by Andreev bound states through the junction with zero resistance. I_c requires coherent charge transport across the semiconductor region and is therefore a measure of both interface transparency and 2DEG mobility.

The junction is neither clearly ballistic ($l_e \gg d$) nor diffusive ($d \gg l_e$), since the mean free path $l_e \approx 370$ nm is of the order of the contact separation. The mean free path is obtained from the transport measurements in a van der Pauw geometry presented earlier. Using the diffusive expression for the Thouless energy $E_T = \hbar D/d^2$ with D being the diffusion constant, we find $E_T \approx 1.1$ meV. This value, which is likely underestimated, since our junction is not deeply diffusive, is about 5 times larger than the superconducting gap Δ_{Al} = 210 μeV, which we extract from the BCS relation $\Delta_{Al} = 1.75k_BT_c$ (see Supporting Information). As a consequence, our junction is close to the short limit.

The Andreev process that carries the supercurrent across the InAsSb semiconductor region is characterized by the induced gap Δ_{ind} in the semiconductor below the Al superconductor, rather than the bulk Al gap, Δ_{Al}. To characterize a superconductor−semiconductor−superconductor junction in the short limit, the product of the critical current and the normal state resistance, which is related to the gap via $I_cR_N = \eta\Delta_{Al}/e$, is often used, where η is a constant of order unity. Experimentally, we find I_cR_N = 270 μV, where I_c = 1.16 μA and R_N = 230 Ω, in the junction with d = 500 nm contact separation at T = 20 mK, consistent with previous results in InAsSb nanowires.[3] The product of I_cR_N can be compared to theoretical values for fully transparent junctions in the short ballistic and short diffusive limits, for which η is π and $1.32(\pi/2)$, respectively.[27] For our sample, we find I_cR_N is 37% of the ballistic limit and 57% of the diffusive limit. This results are comparable with what has been observed in InAs 2DEG for similar contact separations.[28]

Due to the high mobility of the $InAs_{0.5}Sb_{0.5}$ channel, the supercurrent persists at longer separations. At d = 1 μm separation, we still observe a substantial supercurrent I_c = 570 nA with I_cR_N = 280 μV; raw data is presented in the Supporting Information.

High interface transparency corresponds to a high probability of Andreev reflection at the interface. Since the semiconductor extends under the superconducting regions, the interface between the two should be highly transparent due to the large area of contact and in situ epitaxial Al growth.[29] The Andreev process that carries supercurrent across the semiconductor region is characterized by the excess current $I_{ex} = I - V/R_N$ through the junction. Excess current does not require coherent charge transport across the junction, as it follows

https://dx.doi.org/10.1021/acsaelm.0c00269
ACS Appl. Electron. Mater. XXXX, XXX, XXX−XXX

simply from charge conservation at the superconductor−semiconductor interfaces. I_{ex} can be calculated by extrapolating from the high-current normal regime to zero voltage as shown in Figure 4b with a dotted line. The excess current in our sample is found to be $I_{ex} = 1\ \mu A$.

When considering interface quality, the more relevant quantity is the product $I_{ex}R_N$. The product $I_{ex}R_N$ can be compared to the superconducting gap with the relation $I_{ex}R_N = \eta'\Delta_{Al}/e$. In the case of a fully transparent superconductor−semiconductor interface, $\eta' = 1.467$ for a diffusive junction[30] and $\eta' = 8/3$ for a ballistic junction. For our sample, $I_{ex}R_N = 230\ \mu V$, which is close to values reported in InAs 2DEG.[28] This value is 35% of the ballistic limit and 65% of the diffusive value for our 500 nm JJ. The Octavio-Tinkham-Blonder-Klapwijk theory allows the ratio $I_{ex}R_N/\Delta$ to be linked to the interface transparency. Using eq 25 of ref 31, we can extract the effective scattering parameter $Z = 0.58$, leading to a 75% probability of Andreev reflection at zero energy. This value is similar to transparencies observed in InAs nanowires.[32]

In conclusion, we have demonstrated a robust superconducting proximity effect in two-dimensional epitaxial Al−$InAs_{0.5}Sb_{0.5}$ systems. Using an optimized MBE growth, we have achieved both high electron mobilities in $InAs_{0.5}Sb_{0.5}$ and successful epitaxial growth of thin film Al. Theoretically expected transport properties were confirmed in the normal and superconducting state by Shubnikov-de Haas oscillations and current−voltage measurements, which establish strong spin−orbit coupling and large critical current in Josephson junctions. Remarkably, the latter property, made possible by high interface transparency, is consistent with a large proximity-induced superconducting gap of ∼270 μeV in $InAs_{0.5}Sb_{0.5}$. The supercurrent between two Al contacts can be sustained in $InAs_{0.5}Sb_{0.5}$ across at least 1000 nm.

While these results clearly indicate that $InAs_{0.5}Sb_{0.5}$-based junctions provide a suitable platform in which to explore topological superconductivity, they also have broader implications. We expect that spin−orbit coupling in $InAs_{0.5}Sb_{0.5}$ could be further controlled through electrostatic gating or magnetic structures to modify quantum transport both in the normal and superconducting state.

■ ASSOCIATED CONTENT

Supporting Information

The Supporting Information is available free of charge at https://pubs.acs.org/doi/10.1021/acsaelm.0c00269.

Temperature dependence of supercurrent and I_cR_N products; characterization of supercurrent in 1 μm Josephson junction (PDF)

■ AUTHOR INFORMATION

Corresponding Author

Javad Shabani − *Center for Quantum Phenomena, Department of Physics, New York University, New York, New York 10003, United States;* orcid.org/0000-0002-0812-2809; Email: jshabani@nyu.edu

Authors

William Mayer − *Center for Quantum Phenomena, Department of Physics, New York University, New York, New York 10003, United States*

William F. Schiela − *Center for Quantum Phenomena, Department of Physics, New York University, New York, New York 10003, United States*

Joseph Yuan − *Center for Quantum Phenomena, Department of Physics, New York University, New York, New York 10003, United States*

Mehdi Hatefipour − *Center for Quantum Phenomena, Department of Physics, New York University, New York, New York 10003, United States*

Wendy L. Sarney − *US Army Combat Capabilities Command, Army Research Laboratory, Adelphi, Maryland 20783, United States*

Stefan P. Svensson − *US Army Combat Capabilities Command, Army Research Laboratory, Adelphi, Maryland 20783, United States*

Asher C. Leff − *US Army Combat Capabilities Command, Army Research Laboratory, Adelphi, Maryland 20783, United States*

Tiago Campos − *Department of Physics, University at Buffalo, State University of New York, Buffalo, New York 14260, United States*

Kaushini S. Wickramasinghe − *Center for Quantum Phenomena, Department of Physics, New York University, New York, New York 10003, United States*

Matthieu C. Dartiailh − *Center for Quantum Phenomena, Department of Physics, New York University, New York, New York 10003, United States*

Igor Žutić − *Department of Physics, University at Buffalo, State University of New York, Buffalo, New York 14260, United States*

Complete contact information is available at: https://pubs.acs.org/10.1021/acsaelm.0c00269

Author Contributions

W.M. and M.H. performed the measurements and analysis, and J.Y. and M.C.D. helped with fabrication of the devices with J.S. providing input. K.S.W. and J.S. designed the stack. W.L.S. and S.P.S grew the epitaxial Al/InAs heterostructures. A.C.L. performed TEM analysis. T.C. developed the simulation model and carried out the simulations. J.S. conceived the experiment. All authors contributed to interpreting the data. The manuscript was written by W.M., W.F.S., M.C.D., I.Ž., and J.S. with suggestions from all the other authors.

Notes

The authors declare no competing financial interest.

■ ACKNOWLEDGMENTS

NYU team acknowledges support from NSF DMR 1836687 and US Army research office grant number W911NF1810067. SUNY Buffalo team acknowledges support form US ONR N000141712793, NSF ECCS-1810266, and the University at Buffalo Center for Computational Research. J.Y. acknowledges funding from the ARO/LPS QuaCGR fellowship reference W911NF1810067.

■ REFERENCES

(1) Žutić, I.; Matos-Abiague, A.; Scharf, B.; Dery, H.; Belashchenko, K. Proximitized materials. *Mater. Today* **2019**, *22*, 85−107.

(2) Alicea, J. New directions in the pursuit of Majorana fermions in solid state systems. *Rep. Prog. Phys.* **2012**, *75*, No. 076501.

(3) Sestoft, J. E.; Kanne, T.; Gejl, A. N.; von Soosten, M.; Yodh, J. S.; Sherman, D.; Tarasinski, B.; Wimmer, M.; Johnson, E.; Deng, M.; Nygård, J.; Jespersen, T. S.; Marcus, C. M.; Krogstrup, P. Engineering

hybrid epitaxial InAsSb/Al nanowires for stronger topological protection. *Phys. Rev. Materials* **2018**, *2*, No. 044202.
(4) Aasen, D.; Hell, M.; Mishmash, R. V.; Higginbotham, A.; Danon, J.; Leijnse, M.; Jespersen, T. S.; Folk, J. A.; Marcus, C. M.; Flensberg, K.; Alicea, J. Milestones Toward Majorana-Based Quantum Computing. *Phys. Rev. X* **2016**, *6*, No. 031016.
(5) Lutchyn, R. M.; Bakkers, E. P. A. M.; Kouwenhoven, L. P.; Krogstrup, P.; Marcus, C. M.; Oreg, Y. Majorana zero modes in superconductor-semiconductor heterostructures. *Nature Reviews Materials* **2018**, *3*, 52−68.
(6) Zhang, H.; Liu, D. E.; Wimmer, M.; Kouwenhoven, L. P. Next steps of quantum transport in Majorana nanowire devices. *Nat. Commun.* **2019**, *10*, 5128.
(7) Serra, L. m. c.; Delfanazari, K. Evidence for Majorana phases in the magnetoconductance of topological junctions based on two-dimensional electron gases. *Phys. Rev. B: Condens. Matter Mater. Phys.* **2020**, *101*, 115409.
(8) Mayer, W.; Dartiailh, M. C.; Yuan, J.; Wickramasinghe, K. S.; Matos-Abiague, A.; Žutić, I.; Shabani, J. Phase signature of topological transition in Josephson Junctions. *arXiv e-prints* **2019**, arXiv:1906.01179.
(9) Fornieri, A.; Whiticar, A. M.; Setiawan, F.; Portolés, E.; Drachmann, A. C. C.; Keselman, A.; Gronin, S.; Thomas, C.; Wang, T.; Kallaher, R.; Gardner, G. C.; Berg, E.; Manfra, M. J.; Stern, A.; Marcus, C. M.; Nichele, F. Evidence of topological superconductivity in planar Josephson junctions. *Nature* **2019**, *569*, 89−92.
(10) Ren, H.; Pientka, F.; Hart, S.; Pierce, A. T.; Kosowsky, M.; Lunczer, L.; Schlereth, R.; Scharf, B.; Hankiewicz, E. M.; Molenkamp, L. W.; Halperin, B. I.; Yacoby, A. Topological superconductivity in a phase-controlled Josephson junction. *Nature* **2019**, *569*, 93−98.
(11) Winkler, G. W.; Wu, Q.; Troyer, M.; Krogstrup, P.; Soluyanov, A. A. Topological Phases in $InAs_{1-x}Sb_x$: From Novel Topological Semimetal to Majorana Wire. *Phys. Rev. Lett.* **2016**, *117*, No. 076403.
(12) Campos, T.; Toloza Sandoval, M. A.; Diago-Cisneros, L.; Sipahi, G. M. Electrical tuning of helical edge states in topological multilayers. *J. Phys.: Condens. Matter* **2019**, *31*, 495501.
(13) Vurgaftman, I.; Meyer, J. á.; Ram-Mohan, L. á. Band parameters for III−V compound semiconductors and their alloys. *J. Appl. Phys.* **2001**, *89*, 5815−5875.
(14) Webster, P.; Riordan, N.; Liu, S.; Steenbergen, E.; Synowicki, R.; Zhang, Y.-H.; Johnson, S. Measurement of InAsSb bandgap energy and InAs/InAsSb band edge positions using spectroscopic ellipsometry and photoluminescence spectroscopy. *J. Appl. Phys.* **2015**, *118*, 245706.
(15) Campos, T.; Faria Junior, P. E.; Gmitra, M.; Sipahi, G. M.; Fabian, J. Spin-orbit coupling effects in zinc-blende InSb and wurtzite InAs nanowires: Realistic calculations with multiband k· p method. *Phys. Rev. B: Condens. Matter Mater. Phys.* **2018**, *97*, 245402.
(16) Betti, M. G.; Corradini, V.; Bertoni, G.; Casarini, P.; Mariani, C.; Abramo, A. Density of states of a two-dimensional electron gas at semiconductor surfaces. *Phys. Rev. B: Condens. Matter Mater. Phys.* **2001**, *63*, 155315.
(17) Winkler, R. *Spin-orbit Coupling Effects in Two-Dimensional Electron and Hole Systems*; Springer Tracts in Modern Physics 191; Springer, 2003.
(18) Tadjine, A.; Niquet, Y.-M.; Delerue, C. Universal behavior of electron g-factors in semiconductor nanostructures. *Phys. Rev. B: Condens. Matter Mater. Phys.* **2017**, *95*, 235437.
(19) Toloza Sandoval, M A; de Andrada e Silva, E A; Ferreira da Silva, A; La Rocca, G C Electron g factor anisotropy in asymmetric III−V semiconductor quantum wells. *Semicond. Sci. Technol.* **2016**, *31*, 115008.
(20) Qu, F.; van Veen, J.; de Vries, F. K.; Beukman, A. J. A.; Wimmer, M.; Yi, W.; Kiselev, A. A.; Nguyen, B.-M.; Sokolich, M.; Manfra, M. J.; Nichele, F.; Marcus, C. M.; Kouwenhoven, L. P. Quantized Conductance and Large g-Factor Anisotropy in InSb Quantum Point Contacts. *Nano Lett.* **2016**, *16*, 7509−7513.
(21) Momma, K.; Izumi, F. *VESTA3* for three-dimensional visualization of crystal, volumetric and morphology data. *J. Appl. Crystallogr.* **2011**, *44*, 1272−1276.
(22) Svensson, S. P.; Sarney, W. L.; Hier, H.; Lin, Y.; Wang, D.; Donetsky, D.; Shterengas, L.; Kipshidze, G.; Belenky, G. Band gap of $InAs_{1-x}Sb_x$ with native lattice constant. *Phys. Rev. B: Condens. Matter Mater. Phys.* **2012**, *86*, 245205.
(23) Belenky, G.; Donetsky, D.; Kipshidze, G.; Wang, D.; Shterengas, L.; Sarney, W. L.; Svensson, S. P. Properties of unrelaxed InAs1-XSbX alloys grown on compositionally graded buffers. *Appl. Phys. Lett.* **2011**, *99*, 141116.
(24) Sarney, W. L.; Svensson, S. P.; Wickramasinghe, K. S.; Yuan, J.; Shabani, J. Reactivity studies and structural properties of Al on compound semiconductor surfaces. *J. Vac. Sci. Technol., B: Nanotechnol. Microelectron.: Mater., Process., Meas., Phenom.* **2018**, *36*, No. 062903.
(25) Suchalkin, S.; Ludwig, J.; Belenky, G.; Laikhtman, B.; Kipshidze, G.; Lin, Y.; Shterengas, L.; Smirnov, D.; Luryi, S.; Sarney, W. L.; Svensson, S. P. Electronic properties of unstrained unrelaxed narrow gap InAsxSb1-xalloys. *J. Phys. D: Appl. Phys.* **2016**, *49*, 105101.
(26) Dedigama, A. R.; Jayathilaka, D.; Gunawardana, S. H.; Murphy, S. Q.; Edirisooriya, M.; Goel, N.; Mishima, T. D.; Santos, M. B. Measurement of the Dresselhaus and Rashba Spin-Orbit Coupling Via Weak Anti-Localization in InSb Quantum Wells. *Narrow Gap Semiconductors* **2008**, *119*, 35−38.
(27) Likharev, K. K. Superconducting Weak Links. *Rev. Mod. Phys.* **1979**, *51*, 101.
(28) Mayer, W.; Yuan, J.; Wickramasinghe, K. S.; Nguyen, T.; Dartiailh, M. C.; Shabani, J. Superconducting proximity effect in epitaxial Al-InAs heterostructures. *Appl. Phys. Lett.* **2019**, *114*, 103104.
(29) Kjaergaard, M.; Nichele, F.; Suominen, H. J.; Nowak, M. P.; Wimmer, M.; Akhmerov, A. R.; Folk, J. A.; Flensberg, K.; Shabani, J.; Palmstrøm, C. J.; Marcus, C. M. Quantized conductance doubling and hard gap in a two-dimensional semiconductor−superconductor heterostructure. *Nat. Commun.* **2016**, *7*, 12841.
(30) Kulik, I. O.; Omel'yanchuk, A. N. Contribution to the microscopic theory of the Josephson effect in superconducting bridges. *JETP Lett.* **1975**, *21*, 96.
(31) Niebler, G.; Cuniberti, G.; Novotný, T. Analytical calculation of the excess current in the Octavio-Tinkham-Blonder-Klapwijk theory. *Supercond. Sci. Technol.* **2009**, *22*, No. 085016.
(32) Gharavi, K.; Holloway, G. W.; LaPierre, R. R.; Baugh, J. Nb/InAs nanowire proximity junctions from Josephson to quantum dot regimes. *Nanotechnology* **2017**, *28*, No. 085202.

https://dx.doi.org/10.1021/acsaelm.0c00269
ACS Appl. Electron. Mater. XXXX, XXX, XXX−XXX